

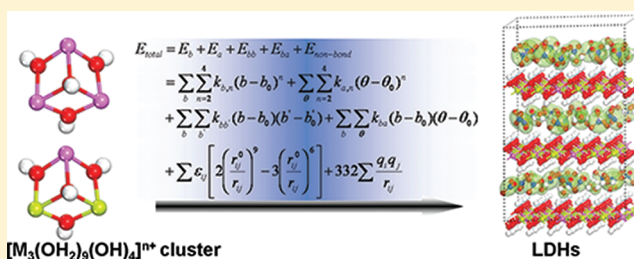
Valence Force Field for Layered Double Hydroxide Materials Based on the Parameterization of Octahedrally Coordinated Metal Cations

Shi-Tong Zhang, Hong Yan,* Min Wei,* David G. Evans, and Xue Duan

State Key Laboratory of Chemical Resource Engineering, Beijing University of Chemical Technology, Beijing 100029, China

Supporting Information

ABSTRACT: A valence force field named LDHFF was systematically developed for the layered double hydroxide (LDH) materials. Its potential function was referred from the polymer consistent force field (PCFF) by introducing a double-well potential to describe the oxygen–metal–oxygen (O–M–O) bending in the octahedral host sheets. The bonded (intramolecular) parameters, including the bond stretching constants, angle bending coefficients, as well as cross terms, were obtained from density function theory (DFT) calculations on the simplified but representative cluster models $[M^{II}_2M^{III}(\text{OH}_2)_9(\text{OH})_4]^{3+}$ and $[M^{III}_3(\text{OH}_2)_9(\text{OH})_4]^{5+}$ ($M^{II}_2M^{III} = \text{Mg}_2\text{Al}, \text{Zn}_2\text{Al}, \text{Co}_2\text{Al}, \text{Ni}_2\text{Al}, \text{Cu}_2\text{Al}, \text{Mg}_2\text{Fe}, \text{Zn}_2\text{Fe}, \text{Ni}_2\text{Fe}, \text{Mg}_2\text{Cr}, \text{Zn}_2\text{Cr}, \text{Cu}_2\text{Cr}, \text{Co}_2\text{Cr}$; $M^{III} = \text{Al}, \text{Fe}, \text{Cr}$). In the case of nonbonded potential, the van der Waals parameters were obtained by fitting them to the cluster models mentioned above. The partial charges used to calculate the Coulombic interactions were assigned as Mulliken charge from density functional theory (DFT) calculation. To validate these potential parameters, a series of molecular dynamics (MD) simulations were subsequently employed for 24 LDH models, and the resulting structures, vibrational frequencies, as well as binding energies are in high accordance with the experimental findings. Using LDHFF, stable octahedral host structures were maintained over 2 ns in molecular dynamics simulations. These results demonstrate that LDHFF works effectively and accurately for MD studies of LDH materials, which provides a theoretical insight for understanding the structural property and exploiting the fabrication of functional LDH and related materials.



1. INTRODUCTION

Layered double hydroxides, also known as anionic clays and hydroxalite-like materials (HTLcs), are a class of minerals and synthetic materials represented by a general formula $[M^{II}_{1-x}M^{III}_x(\text{OH})_2]^{x+} \cdot (A^{n-})_{x/n} \cdot m\text{H}_2\text{O}$, where M^{II} and M^{III} are metal cations that occupy octahedral positions in hydroxide layers; x is the molar ratio $M^{II}/(M^{II}+M^{III})$; and A denotes interlayer charge-compensating anions. The structure of layered double hydroxides (LDHs) is based on a stacking of alternating positively charged metal hydroxide (brucite-type) layers and negatively charged anions and water molecules.^{1,2} Frequently observed M^{II} and M^{III} species include Mg^{2+} , Zn^{2+} , Co^{2+} , Ni^{2+} , Cu^{2+} , Ca^{2+} , etc. and Al^{3+} , Fe^{3+} , and Cr^{3+} , etc., respectively.^{3,4} LDHs are one family of important layered materials which represents a large versatility in terms of chemical composition and capability to build up 2D-organized structures (stacking of the host layers gives rise to an accessible interlayer space in the nanometer scale).⁵ Therefore, they have attracted considerable attention in both fundamental investigations and technological applications including catalysis and adsorption,^{6a} gene and molecular reservoir,^{6b} optical materials,^{6c} functional hybrid additives,^{6d} and controlled drug-release systems.^{6e}

Although LDH materials have been widely used in various fields, detailed information and understanding of their structures are rather insufficient owing to the limitation of experimental techniques. This leads to difficulties in the design

and fabrication of advanced functional LDH materials from the viewpoint of structure–property correlation.^{4,7,8} With the development of computational technologies, molecular dynamics (MD) simulations have been increasingly employed to understand the microstructure and property of LDHs combined with experimental measurements in the past decades.⁷ The energy of a system in MD simulation is calculated by a force field (FF, potential function), which includes various parameters accounting for the interactions of all atoms in a modeled system. The efficiency and accuracy of a FF play a key role in the success of MD simulation.⁹ A large number of force fields, such as Dreiding force field,¹⁰ universal force field (UFF),¹¹ Compass,¹² and consistent force field (CFF),¹³ have been developed for different material systems. As for LDH simulation, a modified Dreiding force field⁴ and ClayFF force field^{14,15} are mostly used. The former was explored by Newman et al., who introduced a harmonic cosine function into Dreiding to model angle bending terms in LDHs, aiming at reducing the distortion of the hydroxide octahedral.⁴ However, the structural distortions were found to be inevitable in their MD simulations,⁴ as a result of the deficiency of the harmonic cosine function in presenting two minima when the

Received: November 21, 2011

Revised: January 12, 2012

Published: January 12, 2012

angle of oxygen–metal–oxygen (O–M–O) in the host layer is close to 90° and 180°, respectively. The latter (ClayFF) was originally designed by Cygan et al.¹⁴ for modeling clay materials, which relies basically on van der Waals and Coulombic interactions instead of covalent bonds to maintain the coordination configurations of central metal cations (either tetrahedral or octahedral). Such a nonbonded model can be directly embedded into other well-developed force fields and shows high computational efficiency. However, Lin et al. pointed out that central metal atoms might escape from the coordination center with a nonbonded type force field in a long-time dynamic simulation.^{16a} Additionally, the simulation results of this nonbonded model are sensitive to the choice of atomic charge models, which impacts the transferability and compatibility.^{16a,b}

Recently, increasing attention has been paid to the LDH materials containing various transition metal cations including Cu, Fe, Co, Cr, etc., due to their excellent performances in catalysis, environment, and energy fields.^{17,18} The force fields mentioned above can not meet the requirement of the fast evolution of LDH materials, because only few metal cations (Mg²⁺, Zn²⁺, and Al³⁺)^{19,20} have been involved in the MD simulation until now. Therefore, a force field including enough parameters for various cations in the octahedral coordination of LDHs is much needed. Adding appropriate parameters to the force field of Newman or Cygan is a possible method, but this approach may cause inevitable distortions owing to their insufficiency of the potential functions. Teppen et al. designed a “double-well” potential in 1997 to describe the octahedral coordination configurations in minerals.²¹ This potential has two minima on its potential energy surface, which is essential for modeling the O–M–O angles in the octahedral sheets of LDHs. All of these inspire us to take the challenge of developing a new force field for LDH systems, which shows superiority in describing the octahedral host layers: including enough parameters for various metal cations and maintaining the structural stability in long-time MD simulation.

In the present work, we developed a force field for LDH materials (denoted as LDHFF), which involves the parameters of all the atoms in the host sheets of LDHs including metal cations, bridging oxygen atoms, as well as hydroxyl hydrogen. The potential function of the polymer consistent force field^{22–25} (PCFF) was employed in this study with the introduction of a double-well potential to model O–M–O bendings, which exhibits excellent performance in reproducing the octahedral coordination. The bonded (intramolecular) parameters for modeling host sheets were derived from density function theory (DFT) calculations on the simplified but representative cluster models. The nonbonded parameters were developed by fitting them to the cluster models and metal hydroxides with brucite-like structure. The resulting force field, LDHFF, was subsequently applied to simulate 24 LDH models with different layer and interlayer composition, to check the transferability of the force field. It was found that the simulated 3D lattice parameters, the calculated vibrational frequencies, as well as the relative binding energies of different anions are in accordance with the experimental results. Moreover, the octahedral structure of the host sheets was observed to be nicely maintained during a long time simulation. These results demonstrate that LDHFF is accurate and efficient in calculating the microstructures and frequencies of LDHs. Therefore, this work provides a fundamental method for understanding the microstructure of LDH materials beyond experimental

techniques, which will give instructions in the exploitation and investigation of functional LDHs and related materials.

2. METHODS

Potential Energy Functions. First of all, we intend to develop a valence force field to avoid the defaults of nonbonded potentials mentioned above. Since PCFF has a robust functional form which has been demonstrated in MD simulations for several kinds of materials,^{21,24–27} its potential function was employed in this study. This allows not only the incorporation of double-well potential but also the availability of the parameters in PCFF to model the interlayer species of LDHs. The potential function of the PCFF force field is

$$E_{\text{total}} = E_b + E_a + E_t + E_{\text{oop}} + E_{bb} + E_{ba} + E_{aa} + E_{bt} + E_{at} + E_{aat} + E_{\text{vdw}} + E_{\text{Coul}} \quad (1)$$

where

$$E_b = \sum_b \sum_{n=2}^4 k_{b,n} (b - b_0)^n \quad (2)$$

$$E_a = \sum_{\theta} \sum_{n=2}^4 k_{a,n} (\theta - \theta_0)^n \quad (3)$$

$$E_t = \sum_{\phi} \sum_{n=1}^3 V_n [1 - \cos(n\phi - \phi_0)] \quad (4)$$

$$E_{\text{oop}} = \sum_{\chi} k_{\chi} (\chi - \chi_0)^2 \quad (5)$$

$$E_{bb} = \sum_b \sum_{b'} k_{bb'} (b - b_0)(b' - b'_0) \quad (6)$$

$$E_{ba} = \sum_b \sum_{\theta} k_{ba} (b - b_0)(\theta - \theta_0) \quad (7)$$

$$E_{aa} = \sum_a \sum_{a'} k_{aa'} (\theta - \theta_0)(\theta' - \theta'_0) \quad (8)$$

$$E_{bt} = \sum_b \sum_{\phi} (b - b_0) \sum_{n=1}^3 V_n [1 - \cos(n\phi - \phi_0)] \quad (9)$$

$$E_{at} = \sum_{\theta} \sum_{\phi} (\theta - \theta_0) \sum_{n=1}^3 V_n [1 - \cos(n\phi - \phi_0)] \quad (10)$$

$$E_{aat} = \sum_{\theta} \sum_{\theta'} \sum_{\phi} k_{\theta\theta'\phi} (\theta - \theta_0)(\theta' - \theta'_0) \cos \phi \quad (11)$$

$$E_{\text{vdw}} = \sum \varepsilon_{ij} \left[2 \left(\frac{r_{ij}^0}{r_{ij}} \right)^9 - 3 \left(\frac{r_{ij}^0}{r_{ij}} \right)^6 \right] \quad (12)$$

and

$$E_{\text{Coul}} = 332.1 \sum \frac{q_i q_j}{r_{ij}} \quad (13)$$

The total energy is divided into three categories: (i) contributions from each of the internal valence coordinates (E_b , E_a , E_ν and E_{oop}), (ii) cross-coupling terms between internal coordinates (E_{bb} , E_{ba} , E_{aa} , $E_{b\nu}$, $E_{a\nu}$ and $E_{aa\nu}$), and (iii) nonbonded interactions (E_{vdw} and E_{Coul}). The valence energies consist of bond stretching term E_b , angle bending term E_a , torsion term E_ν and out-of-plane bending term E_{oop} . The torsion term E_ν was neglected when simulating metal cations because the torsion expression allows at most 3-fold periodicity, but four minima are needed at octahedral centers (the dihedral angle, oxygen–metal–oxygen–metal, has four minimum values near 0° , 90° , 180° , and 270° , respectively). Three cross terms, $E_{b\nu}$, $E_{a\nu}$ and $E_{aa\nu}$ involving torsion interactions were consequently ignored in this study. Another cross term E_{aa} was also neglected because the double-well function was employed to model angle bending terms, which actually involves the coupling interactions between two neighbor O–M–O angles. The out-of-plane bending term E_{oop} was not necessary⁹ and thus neglected. The nonbonded energies are subsequently divided into short-range van der Waals interactions E_{vdw} and long-range Coulombic interactions E_{Coul} . A Lennard-Jones (9-6) function²³ was used to represent the van der Waals energy with a sixth power combination between $r_{ij}^0 = ((r_i^6 + r_j^6)/2)^{1/6}$ and $\varepsilon_{ij} = (\varepsilon_i \varepsilon_j)^{1/2} [2r_i^3 r_j^3 / (r_i^6 + r_j^6)]$, where r_i , r_j , ε_i , and ε_j are the empirical parameters obtained by fitting the model to the observed structural and physical property data. More detailed physical explanations of the parameters in eqs 1–13 are described in the Supporting Information.

Consequently, the potential function of the force field, LDHFF, can be described as

$$E_{\text{total}} = E_b + E_a + E_{bb} + E_{ba} + E_{\text{vdw}} + E_{\text{Coul}} \quad (14)$$

It is noteworthy that the double-well angle bending potential adopted for describing O–M–O angles (θ) is as follow

$$E_a = -\frac{\pi^2}{8} k_{a,4} \left(\theta - \frac{3\pi}{4} \right)^2 + k_{a,4} \left(\theta - \frac{3\pi}{4} \right)^4 \quad (15)$$

Equation 15 was derived from eq 3, which displays dual minima at 90° and 180° to maintain the octahedral geometry.²¹

2.2. Cluster Models for Calculating Potential Parameters. The parameters of a force field can be derived from either experimental data or quantum-mechanical calculations; however, some experimental data of bonded interactions are not available. As a result, DFT calculations on simplified models have been chosen for the development of force fields in the case of complicated systems^{16,26,27} since the results can provide detailed information about the structural properties, vibrational frequencies, and atomic charges, which are necessary for parametrization. In this study, a cluster model was applied to develop the local properties of LDHs, which is a key step in parametrizing the potential: the cluster model should represent the structural features as closely as possible and possess the most economic computer time. Our previous studies have testified that the cluster model with three metal cations represented by $[M^{II}_2 M^{III}(\text{OH}_2)_9(\text{OH})_4]^{3+}$ or $[M^{III}_3(\text{OH}_2)_9(\text{OH})_4]^{5+}$ is the most effective model which includes the basic information of the octahedral coordinated

cations inside the LDH layer.²⁸ A total of 15 such clusters were constructed (Figure 1) including twelve

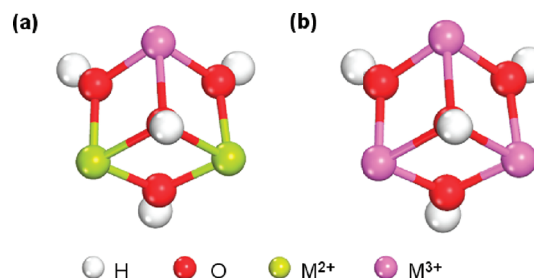


Figure 1. Computational models of (a) $[M^{II}_2 M^{III}(\text{OH}_2)_9(\text{OH})_4]^{3+}$ ($M^{II} M^{III} = \text{Mg}_2\text{Fe}$, Zn_2Fe , Ni_2Fe , Mg_2Cr , Zn_2Cr , Cu_2Cr , Co_2Cr) clusters and (b) $[M^{III}_3(\text{OH}_2)_9(\text{OH})_4]^{5+}$ ($M = \text{Al}$, Fe , Cr) clusters. Only the linkages around the three-centered bridging OH group are displayed for clarification.

$[M^{II}_2 M^{III}(\text{OH}_2)_9(\text{OH})_4]^{3+}$ models ($M^{II} M^{III} = \text{Mg}_2\text{Al}$, Zn_2Al , Co_2Al , Ni_2Al , Cu_2Al , Mg_2Fe , Zn_2Fe , Ni_2Fe , Mg_2Cr , Zn_2Cr , Cu_2Cr , Co_2Cr) and three $[M^{III}_3(\text{OH}_2)_9(\text{OH})_4]^{5+}$ models ($M = \text{Al}$, Fe , Cr), so that different intramolecular packing environments for each metal cation can be taken into consideration. The energy gradient, vibrational frequency, and charge distribution for the parametrization of the force field for LDHs were obtained by the DFT calculation of these clusters. It should be noted that the calculation results of five clusters (Mg_2Al , Zn_2Al , Co_2Al , Ni_2Al , and Cu_2Al) were cited from our previous investigation²⁸ and the remaining 10 models were calculated in this work.

2.3. Models for Molecular Simulations. Molecular simulations were carried out on a series of models with different compositions and structures (Figure 2) for the purpose of validating the LDHFF. Thirteen supercell models were constructed, which can be stoichiometrically expressed in Table 1.

The models of $M(\text{OH})_2$ were established in accordance with their crystal data (Figure 2a).²⁹ The supercell models with molar ratio $M^{II}/M^{III} = 2$ were $6 \times 6 \times 1$ in the a -, b -, and c -direction, respectively, containing 24 divalent metals cations, 12 trivalent cations, and 72 OH groups in each octahedral layer (Figure 2b and 2c). The supercell of $\text{Ni}_3\text{Fe}-\text{CO}_3$ -LDH was constructed as $4 \times 4 \times 1$, which consists of 18 Ni atoms, 6 Fe atoms, and 48 OH groups in each layer (Figure 2d). The layer coordinates of $\text{Zn}_2\text{Al}-\text{CO}_3$ -LDH were determined by Merlino's refinement of X-ray data with $2H$ polytype,³⁰ and the remaining models were constructed using coordinates from the crystal data of the $\text{Mg}_2\text{Al}-\text{CO}_3$ -LDH obtained by Allmann and Jepsen³¹ with $3R$ polytype. Anions and water molecules are intercalated into the interlayer galleries at random positions; the content of the interlayer water in each model was regulated as identically as possible to its given formula.

2.4. Computational Details. The geometries of the cluster models were fully optimized with the DFT method of B3LYP.³² The effective core potentials (ECPs) LanL2DZ were employed for Fe, Cr, and the divalent metal ions, and the full electron basis sets, 6-31+G(d),³³ were used for Al, O, and H. No constraints were imposed on the geometry in any of the DFT computations. The attainment of the energy minimum of each structure in full geometry optimization was tested by frequency calculations. The calculations were performed with the Gaussian 09 program.³⁴

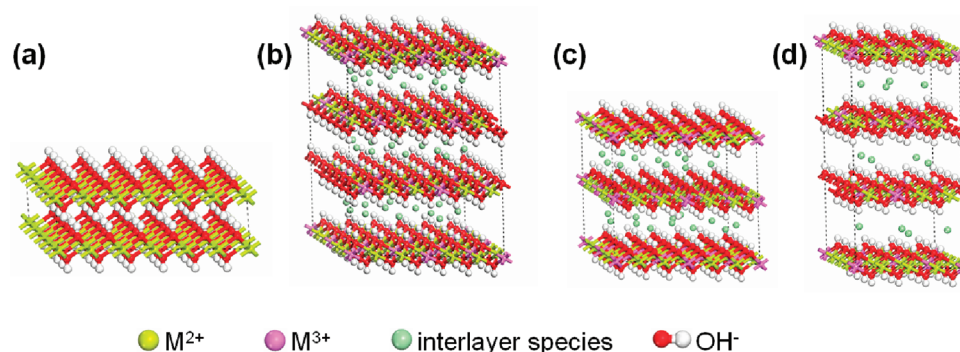


Figure 2. Molecular simulation models of (a) $M(\text{OH})_2$ ($M = \text{Mg}, \text{Zn}, \text{Co}, \text{and Ni}$), (b) LDHs with 3R polytype, (c) LDHs with 2H polytype, and (d) $\text{Ni}_3\text{Fe}-\text{CO}_3\text{-LDH}$.

Table 1. Molecular Formula and Corresponding Abbreviations of the Models Used in Simulations

molecular formula	abbreviation
$M(\text{OH})_2$ ($M = \text{Mg}, \text{Zn}, \text{Co}, \text{and Ni}$)	
$\text{Mg}_{0.67}\text{Al}_{0.33}(\text{OH})_{2.0}(\text{CO}_3)_{0.17}(\text{H}_2\text{O})_{0.5}$	$\text{Mg}_2\text{Al}-\text{CO}_3\text{-LDH}$
$\text{Mg}_{0.67}\text{Al}_{0.33}(\text{OH})_{2.0}(\text{NO}_3)_{0.33}(\text{H}_2\text{O})_{0.22}$	$\text{Mg}_2\text{Al}-\text{NO}_3\text{-LDH}$
$\text{Zn}_{0.67}\text{Al}_{0.33}(\text{OH})_{2.0}(\text{CO}_3)_{0.17}(\text{H}_2\text{O})_{0.50}$	$\text{Zn}_2\text{Al}-\text{CO}_3\text{-LDH}$
$\text{Zn}_{0.67}\text{Al}_{0.33}(\text{OH})_{2.0}\text{Cl}_{0.33}(\text{H}_2\text{O})_{0.67}$	$\text{Zn}_2\text{Al}-\text{Cl-LDH}$
$\text{Co}_{0.67}\text{Al}_{0.33}(\text{OH})_{2.0}(\text{CO}_3)_{0.17}(\text{H}_2\text{O})_{0.42}$	$\text{Co}_2\text{Al}-\text{CO}_3\text{-LDH}$
$\text{Cu}_{0.67}\text{Cr}_{0.33}(\text{OH})_{2.0}\text{Cl}_{0.33}(\text{H}_2\text{O})_{0.67}$	$\text{Cu}_2\text{Cr}-\text{Cl-LDH}$
$\text{Zn}_{0.67}\text{Cr}_{0.33}(\text{OH})_{2.0}\text{Cl}_{0.33}(\text{H}_2\text{O})_{0.67}$	$\text{Zn}_2\text{Cr}-\text{Cl-LDH}$
$\text{Co}_{0.67}\text{Fe}_{0.33}(\text{OH})_{2.0}(\text{CO}_3)_{0.17}(\text{H}_2\text{O})_{0.33}$	$\text{Co}_2\text{Fe}-\text{CO}_3\text{-LDH}$
$\text{Ni}_{0.75}\text{Fe}_{0.25}(\text{OH})_{2.0}(\text{CO}_3)_{0.13}(\text{H}_2\text{O})_{0.50}$	$\text{Ni}_3\text{Fe}-\text{CO}_3\text{-LDH}$

In molecular simulations, the single-point charge (SPC) water model,³⁵ which has been successfully used in other molecular simulations, was used to represent the interlayer water.^{14,36} To maintain the electric neutrality of LDHs, the total charges of interlayer anions were set to be their formula charges, and the partial charge of each atom was derived from Mulliken population analysis of the above-mentioned DFT calculation. The force field parameters for anions originate from the PCFF. The long-range Coulombic interactions among partial charges were computed by the Ewald summation³⁷ technique, and a “spline cutoff” method was used to calculate van der Waals interaction. MD simulations were performed in isothermal–isobaric (*NPT*) ensemble with the temperature of 298 K and the pressure of 0.1 MPa. The Andersen method³⁸ and Parrinello–Rahman³⁹ method were used for controlling temperature and pressure, respectively. The simulation time step was 1 fs, and the total simulation time was 60 ps for each model. The results showed that the system reached equilibrium with lattice parameters and total potential energy fluctuating around a constant value within the first 20 ps (Figure S3, Supporting Information). So dynamic trajectories during the remaining 40 ps were recorded every 10 fs to analyze the ensemble average values, such as the lattice parameters, lengths of metal–oxygen bonds, and interlayer orientations. The 2 ns dynamic simulations were carried out for the $\text{Mg}_2\text{Al}-\text{NO}_3\text{-LDH}$ model to test the validity of the force field in maintaining the octahedral coordination in long-time MD simulations. All of the molecular simulations were performed using the Forcite module in the Material Studio version 5.5 software package (Accelrys Software, Inc.).

3. RESULTS AND DISCUSSION

3.1. Parameterization. To derive parameters for the potential function, the following terms were developed: the stretching constants $k_{b,2}$, $k_{b,3}$, and $k_{b,4}$ and reference bond length b_0 for the M–O bond; the bending constants $k_{a,2}$, $k_{a,3}$, $k_{a,4}$ and reference angle θ_0 for the O–M–O, M–O–M, and M–O–H angles; the coupling constants $k_{bb'}$ and k_{ba} for cross terms; the well depth ϵ ; van der Waals radii r_i^0 ; and partial charge q_i for metal cations.

3.1.1. Parameterization of Bonded Parameters. On the basis of the optimized models, the harmonic parameters $k_{b,2}$, $k_{a,2}$, and the coupling constants $k_{bb'}$ and k_{ba} were derived from the Hessian matrix in Cartesian coordinates (CART). Seminario’s method was used to calculate the harmonic force constants $k_{b,2}$ and $k_{a,2}$ for internal coordinates.^{16,40,41} This method has been successfully employed in many previous reports.^{16,42} $k_{bb'}$ and k_{ba} were obtained from coordinate translations (Supporting Information: Seminario’s method and matrix translations). The force field parameters for H–O, Al–O, and O–Al–O were referred from the reported work.^{21,26,43,44}

Cubic and quartic terms were introduced into the force field to reproduce the anharmonic property of a true bond stretching potential.⁹ Distortions of the equilibrium geometry along internal coordinates were built to fit such anharmonic constants with the least-squares method. The SCF energies, the atom charges, as well as the SCF gradients were calculated. Thirty distorted structures were considered for each cluster models (typically ± 0.1 Å for bond lengths and $\pm 2^\circ$ for bond angles) to fit the energy variation surface. The stretching potential of a true bond rises more quickly as the bond length shrinks from its equilibrium position than that as it expands. This implies that the average value of bond lengths in a vibrating molecule is larger than the equilibrium value, according to the Boltzmann distribution. The reference bond lengths b_0 were optimized, which were slightly larger than their equilibrium values in DFT-optimized structures by 0.1–0.2 Å. These bonded parameters were optimized by the pattern search method.^{45a–c} The cluster models and the $M(\text{OH})_2$ ($M = \text{Mg}, \text{Ni}, \text{Zn}, \text{and Co}$) models were employed to obtain the physical intensities (e.g., the bond lengths of metal–oxygen) used in the optimization. The final intramolecular force field parameters are listed in Table 2.

3.1.2. Parameterization of Nonbonded Parameters. The intermolecular interaction including the van der Waals and Coulombic terms plays a key role in determining the orientation and arrangement of the interlayer species. The parametrization of such nonbonded terms should be performed

Table 2. Developed Bonded Force Field Parameters of LDHFF

bond stretching: $E_{b,ij} = k_{b,2}(b - b_0)^2 + k_{b,3}(b - b_0)^3 + k_{b,4}(b - b_0)^4$				
	b_0 (Å)	$k_{b,2}$ (kcal·mol ⁻¹ ·Å ⁻²)	$k_{b,3}$ (kcal·mol ⁻¹ ·Å ⁻³)	$k_{b,4}$ (kcal·mol ⁻¹ ·Å ⁻⁴)
Mg–O	2.340	61.3	-169.3	187.6
Al–O	2.035	328.7	-341.0	2189.0
Cr–O	1.995	115.0	-183.9	77.0
Fe–O	2.080	94.4	-225.1	187.8
Co–O	2.280	63.0	-162.8	121.5
Ni–O	2.310	71.6	-150.6	141.2
Cu–O	2.340	62.7	-145.6	99.0
Zn–O	2.360	60.2	-354.7	137.1
O–H	0.965	532.5	-1282.0	2004.0
angle bending: $E_{a,ijk} = k_{a,2}(\theta - \theta_0)^2 + k_{a,3}(\theta - \theta_0)^3 + k_{a,4}(\theta - \theta_0)^4$				
	θ_0 (degree)	$k_{a,2}$ (kcal·mol ⁻¹ ·rad ⁻²)	$k_{a,3}$ (kcal·mol ⁻¹ ·rad ⁻³)	$k_{a,4}$ (kcal·mol ⁻¹ ·rad ⁻⁴)
Al–O–Al	104.0	195.5	48.9	185.1
Ni–O–Ni	102.0	83.9	-113.1	0.0
Zn–O–Zn	107.0	82.2	-101.3	0.0
Mg–O–Mg	107.0	83.9	-94.4	0.0
Co–O–Co	102.0	49.5	-50.0	0.0
Fe–O–Fe	102.0	139.0	-269.0	0.0
Cu–O–Cu	108.0	107.3	-245.6	267.7
Cr–O–Cr	107.0	210.2	-338.9	0.0
O–Al–O	135.0	-40.0	0.0	32.4
O–Ni–O	135.0	-42.2	0.0	34.2
O–Zn–O	135.0	-39.5	0.0	32.1
O–Mg–O	135.0	-37.4	0.0	30.3
O–Co–O	135.0	-42.7	0.0	34.7
O–Cr–O	135.0	-23.4	0.0	18.9
O–Cu–O	135.0	-25.1	0.0	20.4
O–Fe–O	135.0	-44.7	0.0	36.2
Al–O–H	121.54	18.0	-14.9	14.7
Ni–O–H	120.0	14.9	-25.6	43.5
Zn–O–H	123.3	4.2	-21.1	61.2
Mg–O–H	121.5	10.6	-11.3	-21.9
Co–O–H	127.0	5.1	-23.8	10.5
Fe–O–H	119.1	12.8	-4.9	0.2
Cu–O–H	125.3	7.2	5.2	15.8
Cr–O–H	119.8	18.9	-29.6	41.8
cross term $E_{rr'} = E_{rr'}(r - r_0)(r' - r'_0)$				
	bond–bond		bond–angle	
	$k_{bb'}$ (kcal·mol ⁻¹ ·Å ⁻²)	k_{ba} (kcal·mol ⁻¹ ·Å ⁻² ·rad ⁻¹)	$k_{b'a}$ (kcal·mol ⁻¹ ·Å ⁻² ·rad ⁻¹)	
Al–O–Al	20.94	-1.328		
Ni–O–Ni	12.25	-2.560		
Zn–O–Zn	18.55	-1.675		
Mg–O–Mg	10.22	-2.904		
Co–O–Co	14.88	-4.131		
Fe–O–Fe	15.44	0.000		
Cu–O–Cu	19.29	-2.101		
Cr–O–Cr	18.13	-1.543		
O–Al–O	15.64	-1.328		
O–Ni–O	20.25	-3.255		
O–Zn–O	15.19	0.469		
O–Mg–O	13.80	-0.227		
O–Co–O	20.63	-3.347		
O–Cr–O	20.65	-1.543		
O–Cu–O	18.04	-1.209		
O–Fe–O	27.63	-1.712		
Al–O–H	5.48	1.224	0.5629	
Ni–O–H	2.90	1.550	0.1940	
Zn–O–H	4.59	0.000	0.2859	
Mg–O–H	2.31	1.475	0.5145	

Table 2. continued

	cross term $E_{rr'} = E_{rr'}(r - r_0)(r' - r'_0)$		
	bond–bond		bond–angle
	$k_{bb'}$ (kcal·mol ⁻¹ ·Å ⁻²)	k_{ba} (kcal·mol ⁻¹ ·Å ⁻² ·rad ⁻¹)	$k_{b'a}$ (kcal·mol ⁻¹ ·Å ⁻² ·rad ⁻¹)
Co–O–H	3.05	0.007	–0.1097
Fe–O–H	3.06	0.430	0.4413
Cu–O–H	5.80	4.500	0.9331

carefully so that the force field parameters of the host atoms can be compatible with those of the guest species which has been independently developed in PCFF. In this study, partial charges of layer atoms were assigned on the basis of Mulliken population analysis for the optimized cluster models $[M^{II}_2M^{III}(\text{OH}_2)_9(\text{OH})_4]^{3+}$ and $[M^{III}_3(\text{OH}_2)_9(\text{OH})_4]^{5+}$ since Mulliken charges have been chosen as the partial charges in many previous reports on MD simulations for LDH materials.^{14,45d} Furthermore, a comparison study between Mulliken charges and RESP charges was also performed, and the results show that Mulliken charges exhibit a better performance (not shown here). We set the partial charge of hydroxyl hydrogen as 0.46 e (average value of different clusters). To keep the electric neutrality, the charge of the bridging oxygen atom was set ranging from –0.80 to –0.70 e. The required Lennard-Jones 9-6 parameters for metal cations were initially set to be the values of octahedral magnesium developed by Cygan.¹⁴ Subsequently, the distance parameter r_0 and energy parameter ϵ_0 were optimized together with the bonded parameters using the pattern search method, until they reproduce the structures of clusters (DFT calculation) and hydroxides (experimental results). During the refinements, the parameters of the oxygen and hydrogen atoms were referred from the original PCFF. This made the obtained parameters harmonize with the original PCFF to give effective and accurate simulation for the LDH systems. The final force field parameters for modeling nonbonded interactions are tabulated in Table 3.

Table 3. Developed Nonbonded Force Field Parameters of LDHFF

nonbonded terms: $E = \epsilon_{ij}[2(r_{ij}^0/r_{ij})^9 - 3(r_{ij}^0/r_{ij})^6] + 332.1(q_i q_j / r_{ij})$			
	r_i (Å)	ϵ_i (kcal/mol)	q_i (e)
Mg	6.300	0.035	0.845
Al	6.200	0.020	1.200
Cr	5.900	0.010	1.250
Fe	6.100	0.300	1.200
Co	6.235	0.028	0.830
Ni	6.010	0.036	0.730
Cu	6.380	0.025	0.700
Zn	6.280	0.020	1.070
Al	3.535	0.240	variable ^a
H	1.098	0.013	0.460

^aThe partial charge of the oxygen atoms is ranging from –0.8 to –0.7 e.

3.2. Validation. 3.2.1. Structures.

To test whether the LDHFF parameters developed for metal cations can be successfully employed in conjunction with the original parameters in PCFF, a series of MD simulations for LDH materials were performed. The common interlayer anions (CO_3^{2-} , Cl^- , and NO_3^-) were chosen in simulation.

As shown in Table 4, each of the calculated supercell parameters, α , β , and γ , was quite close to 90°, 90°, and 120°, respectively, although they were fully relaxed during the simulations with P1 symmetry. The average values of the identical *a*- and *b*-axis length of the unit cell are in good agreement with the experimental data from XRD. Compared with the results simulated by ClayFF¹⁴ or the modified Dreiding force field,¹⁰ LDHFF largely improves the accuracy of structural properties of LDHs. Taking the interlayer distance (d_{001}) as an example (Table 4), the calculated values using LDHFF show a remarkably smaller deviation from the experimental ones than those estimated by Dreiding or ClayFF. The experimental values of the unit cell parameter (*a* or *b*) of LDHs increase in the order: $\text{Mg}_2\text{Al} < \text{Co}_2\text{Al} < \text{Zn}_2\text{Al} < \text{Ni}_3\text{Fe} < \text{Zn}_2\text{Cr} < \text{Cu}_2\text{Cr} < \text{Co}_2\text{Fe}$ –LDHs (Table 4). Our calculation generally reproduces this trend except for Zn_2Cr – and Cu_2Cr –LDH, which show a rather close experimental cell parameter (*a* or *b*) to each other. In fact, Zn^{2+} has a larger radius than that of Cu^{2+} ,⁴⁹ but the experimentally observed parameter *a* of Zn_2Cr –Cl–LDH is slightly smaller than that of Cu_2Cr –Cl–LDH. This suggests that the average value of the O–M–O angle in Zn_2Cr –Cl–LDH is larger than that in Cu_2Cr –Cl–LDH, which was verified by our calculations (Figure S4, Supporting Information).

CO_3^{2-} and NO_3^- have similar trigonal structure and molecular size: the central atom (C or N) is bonded to three O atoms through sp^2 hybrid type, and the ionic radius is around 1.3 Å. However, they produce rather different interlayer distance (7.60 Å for CO_3^{2-} and 8.95 Å for NO_3^-) in Mg_2Al –LDH according to the powder XRD data.^{29,48a} Xu and Zheng experimentally proposed three possible conformations concerning distributions of CO_3^{2-} and NO_3^- in the LDH gallery, the flat-lying model, the tilt-lying model, and the stick-lying model,^{48a} but the exact intercalated styles remain unclear. Here, we studied their intercalated styles by using LDHFF. The results (Table 4) show that the calculated interlayer distances of Mg_2Al –LDH containing CO_3^{2-} and NO_3^- are 7.72 and 8.93 Å, respectively, in accordance with the experimental ones. Figure 3a and 3b are random snapshots from MD simulations of MgAl – CO_3 –LDH and MgAl – NO_3 –LDH after 20 ps, from which it can be visually observed that the interlayer CO_3^{2-} presents a flat-lying style while NO_3^- displays a tilt-lying style. This relates with their different density in the gallery owing to their different charges. The number of interlayer nitrate is twice that of carbonate; as a result, the repulsion between NO_3^- anions is more prominent. NO_3^- thus favors to display a tilt-lying style to minimize the repulsive force and optimize the distribution. The stick-lying style, in which the interlayer anions lay parallel to the host sheets with a double-layer arrangement, was not observed in our simulation. This is reasonable because the interlayer water molecules destroy the hydrogen bonds between oxygen atoms in CO_3^{2-} or NO_3^- and the host layer.

To further validate the transferability of LDHFF, the MgAl – NO_3 –LDH models with $\text{Mg}^{2+}/\text{Al}^{3+}$ molar ratio ranging from

Table 4. Simulated Structures Using LDHFF in Comparison with Experimental Results

	α (deg)	β (deg)	γ (deg)	a, b (Å)		c (Å)		interlayer spacing (Å)			rms ^g (Å)
	calc	calc	calc	calc	exptl	calc	exptl	calc	calc ^a	exptl	
Mg(OH) ₂	90.00	90.00	120.00	18.82	18.88 ²⁹	4.75	4.77 ²⁹	4.75	4.59 ^b	4.77 ²⁹	0.05
β -Co(OH) ₂	90.00	90.00	120.00	18.98	19.12 ^{47a}	4.65	4.65 ^{47a}	4.65		4.65 ^{47a}	0.11
β -Ni(OH) ₂	90.00	90.00	120.00	18.69	18.68 ^{47b}	4.62	4.62 ^{47b}	4.62	4.59 ^c	4.62 ^{47b}	0.01
β -Zn(OH) ₂	90.00	90.00	120.00	19.04	19.16 ^{47c}	4.74	4.71 ^{47c}	4.74		4.71 ^{47c}	0.10
Mg ₂ Al-CO ₃	90.02	89.99	120.02	18.24	18.32 ³¹	23.17	22.81 ³¹	7.72	7.30 ^{d,4}	7.60 ³¹	0.10
Mg ₂ Al-NO ₃	89.82	89.38	120.00	18.27	18.25 ^{48a}	26.78	26.86 ^{48a}	8.93	8.67 ^b	8.95 ^{48a}	0.02
Mg ₃ Al-NO ₃	89.40	89.80	120.05	12.26	12.22 ^{48a}	25.41	25.47 ^{48a}	8.47	8.61 ^{e,4}	8.49 ^{48a}	0.03
Zn ₂ Al-Cl	89.67	90.36	119.99	18.39	18.45 ⁴⁶	22.69	23.15 ⁴⁶	7.56	7.50 ^f	7.72 ⁴⁶	0.10
Zn ₂ Al-CO ₃	90.00	90.00	120.00	18.42	18.44 ³⁰	15.08	15.11 ³⁰	7.54		7.56 ³⁰	0.02
Zn ₂ Cr-Cl	89.97	89.97	120.07	18.67	18.63 ^{48b}	23.23	22.64 ^{48b}	7.74		7.55 ^{48b}	0.11
Co ₂ Al-CO ₃	89.98	89.96	119.97	18.28	18.41 ^{48c}	22.39	22.61 ^{48c}	7.46		7.54 ^{48c}	0.12
Co ₂ Fe-CO ₃	90.03	90.00	119.95	18.73	18.72 ^{48d}	22.56	22.78 ^{48d}	7.52		7.59 ^{48d}	0.04
Cu ₂ Cr-Cl	90.05	89.74	119.99	18.52	18.66 ^{48b}	23.13	23.15 ^{48b}	7.71		7.72 ^{48b}	0.11
Ni ₃ Fe-CO ₃	89.89	89.81	119.96	12.40	12.32 ^{48e}	22.95	23.27 ^{48e}	7.65		7.76 ^{48e}	0.09

^aCalculated value using the ClayFF or Dreiding force field. ^bCalculated value with the ClayFF force field. ^cData from ref 45, calculated by modified CFF91. ^dData of Mg₃Al(OH)₆(CO₃)_{0.5}(H₂O)₂ from ref 4, calculated by the Dreiding force field. ^eData of Mg₃Al(OH)₆NO₃(H₂O)₂ from ref 4, calculated by the Dreiding force field. ^fData from ref 46, calculated by the ClayFF force field. ^gExperimental results were chosen as the reference values.

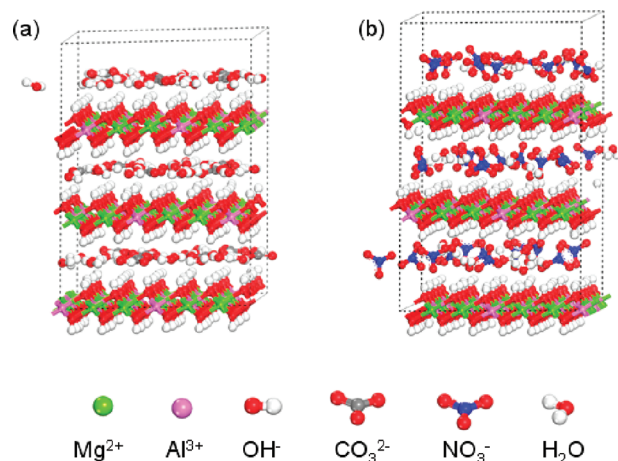


Figure 3. Snapshots of the NPT (298.0 K and 0.1 MPa) MD simulations of (a) Mg₂Al-CO₃-LDH and (b) Mg₂Al-NO₃-LDH. The interlayer CO₃²⁻ presents a flat-lying style, and NO₃⁻ displays a tilt-lying style.

4/2 to 9/2 were calculated, and it was found that the value and the change of simulated interlayer distances agree well with the experimental values (Figure 4).^{48a} As the Mg²⁺/Al³⁺ ratio increases, the interlayer distance decreases gradually until the ratio reaches 7/2 and then rises slightly (Figure 4). The initial decrease of the interlayer spacing is largely attributed to the reduction of the density of interlayer NO₃⁻. Upon further increasing Mg²⁺/Al³⁺ molar ratio from 7/2 to 9/2, the content of interlayer water molecule enhances, which leads to a slightly larger interlayer distance. For comparison, simulations using the nonbonded force field were also carried out for the same system (the force field parameters come mainly from ClayFF, Table S2, Supporting Information). As shown in Figure 4, a relatively large deviation was observed between the simulated interlayer distance and the experimental data for the nonbonded model, especially a serious underestimation by more than 2.0 Å with molar ratio Mg²⁺/Al³⁺ = 3. These results reflect that LDHFF is better than the nonbonded model in the MD studies of LDHs.

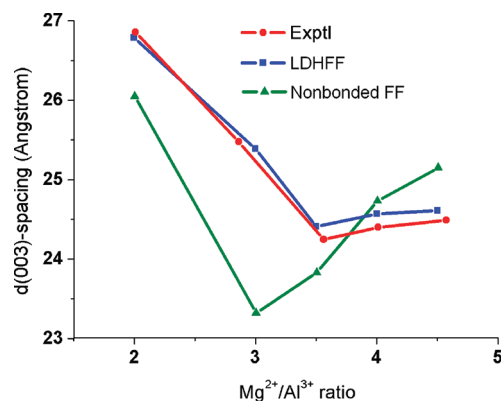


Figure 4. Calculated c parameters of MgAl-LDHs with different Mg²⁺/Al³⁺ ratios by LDHFF (blue line) and nonbonded force field (green line). Experimental results (red line) are also displayed for comparison.

3.2.2. Vibrational Frequencies. We also calculated the vibrational properties of the M(OH)₂ models to validate LDHFF. Vibrational frequencies are obtained from the minimized models using the Hessian matrix.⁵⁰ The possible vibrational modes of a regular crystalline solid can be analyzed using the technique of factor group analysis.^{51,52} For brucite and metal hydroxides with brucite-like structure, the factor group is D_{3d} .^{52,53} The vibrational modes of M(OH)₂ are described in Table S4 (Supporting Information), and the calculated vibrational frequencies of M(OH)₂ compared with experimental results are shown in Table 5. Overall, the calculated vibrational frequencies are in agreement with the experimental results. The largest discrepancy was found in the A_{2u} mode of brucite (455 cm⁻¹ for experiment and 648 cm⁻¹ for calculation). This mode corresponds to the lattice vibrations, in which both the metal cations and the OH groups vibrate along the c -direction. Since most of the force field parameters were derived from the DFT calculation of cluster models, it is reasonable that the lattice vibrational frequencies predicted by force field present hypsochromic (or bathochromic) shifts compared with the experimental results. On the other hand, the

Table 5. Calculated Vibrational Frequencies (in cm^{-1}) of $\text{M}(\text{OH})_2$ in Comparison with Experimental Results

mode		$\text{Mg}(\text{OH})_2$		$\text{Co}(\text{OH})_2$		$\text{Ni}(\text{OH})_2$	
representation	group motion	calc	exptl ⁵⁴	calc	exptl ⁵⁵	calc	exptl ⁵⁵
A_{1g}	OH stretch	3609	3652	3600	3559	3590	3580
A_{2u}	OH stretch	3629	3688	3632	3630	3635	3639
E_g	OH rotation	703	725	748		710	
E_u	OH rotation	387	415	450	433	442	452
A_{1g}	OH translation	492	443	522		513	449
A_{2u}	OH translation	648	455	563	510	552	530
E_g	OH translation	361	280	243		301	318
E_u	cell translation	471	361	303	314	362	350

calculated vibrational frequencies of OH stretching ($A_{1g} + A_{2u}$) and MOH bending ($E_g + E_u$) are rather close to those of experiments. This indicates that the cluster models used to develop the force field parameters can satisfactorily reproduce the local properties of crystals.

Furthermore, the vibrational properties of the interlayer anions were calculated with LDHFF. The model of $\text{Zn}_2\text{Al}-\text{CO}_3$ -LDH was employed because its vibration properties have been fully studied in reported experimental work.⁵⁶ Table 6 lists

Table 6. Calculated Vibrational Frequencies (in cm^{-1}) of Interlayer Carbonate Compared with Experimental Results

vibrational mode	exptl ⁵⁶		calc	
	solution	LDHs	free	LDHs
$\nu_{\text{as,C-O}}$	1415	1416, 1313	1659	1715, 1690
$\nu_{\text{s,C-O}}$		1012	1092	1122
$\gamma_{\text{O-C-O}}$	880	870	918	896
$\delta_{\text{O-C-O}}$	680	670	746	678, 781

the simulated results accompanied with the experimental ones. According to the experiments,⁵⁴ the free carbonate anion has D_{3h} point group symmetry, and its infrared spectra present three bands: the antisymmetric C–O stretching of E' symmetry ($\nu_{\text{as,C-O}}$) at 1415 cm^{-1} , the out-of-plane O–C–O bend of A_2'' symmetry ($\gamma_{\text{O-C-O}}$) at 880 cm^{-1} , and the $\delta_{\text{O-C-O}}$ (E') at 680 cm^{-1} associated with the in-plane O–C–O bending. When the carbonate is intercalated into LDHs, the mode $\nu_{\text{s,C-O}}$ (A_1') related to symmetric C–O stretching becomes IR active at 1012 cm^{-1} , and the $\nu_{\text{as,C-O}}$ mode splits into two bands at 1416 and 1313 cm^{-1} ,⁵⁴ which indicates a low symmetry of the interlayer CO_3^{2-} . It can be seen that the calculated results are generally in accordance with the experimentally observed results except for the $\nu_{\text{as,C-O}}$ mode with a hypsochromic shift. We also employed PCFF to calculate the vibration of a free carbonate and found that the $\nu_{\text{as,C-O}}$ mode mainly occurs at 1659 cm^{-1} . This overestimation may be due to the absence of cross terms in PCFF to describe the carbonate.

3.2.3. Exchange Priority of Interlayer Anions. LDHs containing a variety of anions are generally synthesized by the ion exchange method. It is therefore important to predict the capability of anions to bind with the metal hydroxide layers. In the present work, CO_3^{2-} , OH^- , NO_3^- , Cl^- , and Br^- intercalated MgAl -LDHs were chosen to test whether LDHFF is competent to achieve this prediction. The relative binding energies of these models (the potential energy of NO_3^- intercalated MgAl -LDHs is taken as a reference, Supporting Information, Table S5), which can be used to indicate the relative affinity order of the exchange anions, were calculated as below

$$U_B(A^{n-}) = \left[U(A^{n-}-\text{Mg}_2\text{Al-LDHs}) - U(\text{NO}_3^- - \text{Mg}_2\text{Al-LDHs}) - N_{\text{water}}U(\text{H}_2\text{O}) - N_A U(A) \right] / N_A \quad (16)$$

where U is the potential energy of the model, and N_{water} and N_A are the number of water molecules and anions, respectively. The result shows that the relative binding energy of the interlayer anion decreases in the order: $\text{NO}_3^- > \text{Br}^- > \text{Cl}^- > \text{OH}^- > \text{CO}_3^{2-}$ (Figure 5). This is consistent with the ion-

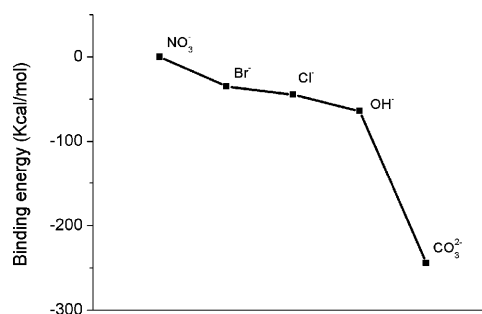


Figure 5. Calculated relative binding energies of different interlayer anions in MgAl -LDHs with LDHFF.

exchange capability of these anions reported by experimental method: $\text{CO}_3^{2-} > \text{OH}^- > \text{Cl}^- > \text{Br}^- > \text{NO}_3^-$.^{3,4,57} The results show that LDHFF can predict the exchange priority of the interlayer anions as expected.

3.3. Long Time MD Simulations on LDHs. When the MD method is used to investigate complicated materials, the simulation must be sufficiently long so that the model can be fully relaxed to its stable structure and displays the most reasonable results. To test the stability of LDHFF in long time MD simulations, we performed a 2 ns dynamic simulation on the $\text{Mg}_2\text{Al}-\text{NO}_3$ -LDH model using LDHFF. Root-mean-square-deviation (rmsd) values of the coordinated metal cations were monitored along the MD trajectory. The results obtained from LDHFF were compared with those of the nonbonded model (the force field parameters are referred to ClayFF; see Table S2, Supporting Information). As displayed in Figure 6a, the MD simulation of the nonbonded model is observed to be structure-broken with sharply increasing rmsd values along its MD trajectory, and six metal cations escaped from their coordination centers in the final structure (Figure 6c). The results show that the nonbonded model does not maintain its structure in the 2 ns simulation, as a result of the substantial attraction between the metal cations and the interlayer anions. In the case of the calculation results by LDHFF, the octahedral

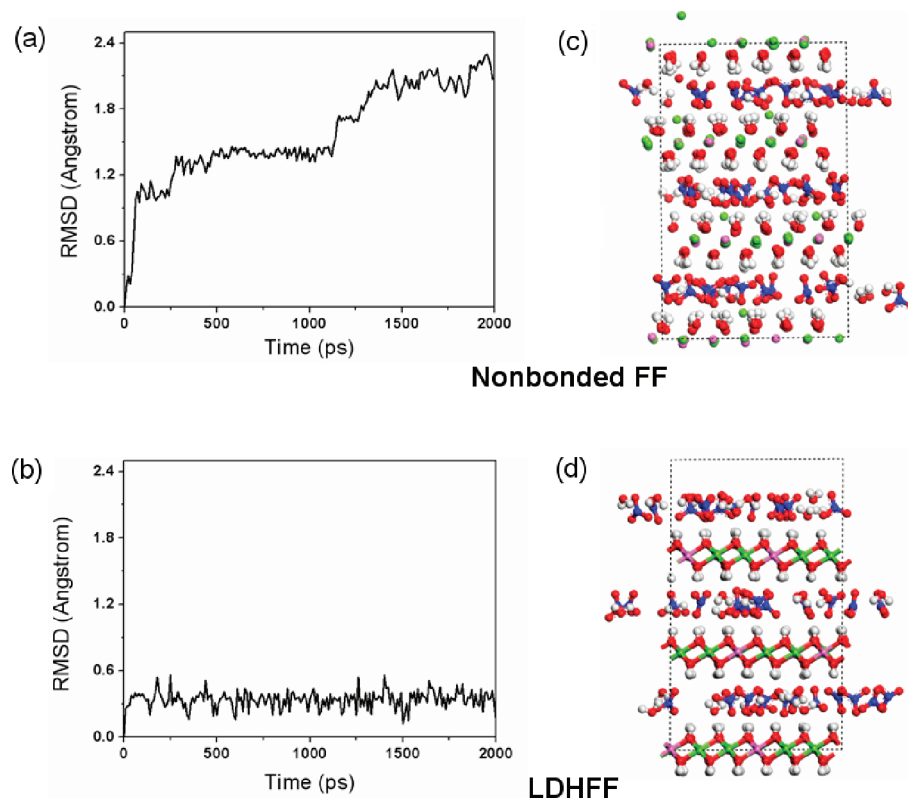


Figure 6. rmsd values of the metal cations in the $\text{Mg}_2\text{Al}-\text{NO}_3$ -LDH models monitored along MD trajectory of (a) the nonbonded FF and (b) LDHFF; the last snapshot of each simulation of (c) the nonbonded FF and (d) LDHFF. The initial structures (Figure S5, Supporting Information) are used as the references.

coordinations in the host layers are nicely maintained during the whole simulation (Figure 6b and 6d). Particularly, the average rmsd value produced by LDHFF is as small as $\sim 0.3 \text{ \AA}$. In the last snapshot on the MD trajectory of LDHFF, the octahedral coordination in the host layers is still maintained. This clearly demonstrates that the LDHFF can produce a more stable structure in long time simulations than the nonbonded potential does, owing to the involvement of both the covalent interaction between M^{n+} and OH^- as well as the double-well potential to describe the O–M–O bendings. Therefore, LDHFF can be effectively applied to investigate LDH materials containing functional interlayer species for the purpose of rational design and theoretical instruction for their fabrication.

4. CONCLUSIONS

A valence force field for LDHs, LDHFF, was systematically developed on the basis of the parametrization of potentials for different kinds of octahedrally coordinated metal cations in the LDH host sheets. The potential function of PCFF was adopted, and the “double-well” potential was introduced for modeling O–M–O bending. A total number of 15 cluster models containing various octahedrally coordinated metal cations ($[\text{M}_3(\text{OH})_9(\text{OH})_4]^{n+}$) were computed at the B3LYP/6-31+G(d)/LanL2DZ level to obtain the desired bonded force field parameters for octahedral Mg^{2+} , Zn^{2+} , Co^{2+} , Ni^{2+} , Cu^{2+} , Al^{3+} , Fe^{3+} , and Cr^{3+} , which are commonly observed for LDHs. In the case of nonbonded potential, the van der Waals parameters were obtained by fitting them to the cluster models and metal hydroxides with brucite-like structure. The partial charges used to calculate the Coulombic interactions were assigned as Mulliken charge from DFT calculation. The refined

parameters were applied in MD simulations to validate LDHFF in terms of structural properties (lattice parameters, interlayer arrangements, $\text{M}^{\text{II}}/\text{M}^{\text{III}}$ molar ratio), vibrational frequencies, binding energies, and stability. It was found that the simulated 3D lattice parameters and calculated vibrational frequencies of the LDH crystals are close to the experimental values; the relative binding energies of different anions are in accordance with their exchange priority. In addition, LDHFF can keep the octahedral structure of the host sheets nicely during long time simulations. This work provides a successful theoretical method which works effectively and accurately for the structural understanding and investigation of LDH-based materials. It is expected that the approach for developing LDHFF can be extended to the development of force fields for other organic–inorganic composite materials based on octahedrally coordinated metals.

■ ASSOCIATED CONTENT

Supporting Information

The optimized geometries, Cartesian coordinates, and total energies of cluster models (Figure S1, Table S1); some geometrical and energetic properties of LDH models in MD simulations by using LDHFF (Figures S2–S5, Tables S2–S5); the seminario’s method and matrix translations. This material is available free of charge via the Internet at <http://pubs.acs.org>.

■ AUTHOR INFORMATION

Corresponding Author

*Tel.: +86-10-64412131. Fax: +86-10-64425385. E-mail: yanhong@mail.buct.edu.cn (Hong Yan); weimin@mail.buct.edu.cn (Min Wei).

Notes

The authors declare no competing financial interest.

ACKNOWLEDGMENTS

This work was supported by the 973 Program (Grant No.: 2011CBA00504), the National Natural Science Foundation of China, the Collaboration Project from the Beijing Education Committee, and the "Chemical Grid Project" of Beijing University of Chemical Technology.

REFERENCES

- (1) (a) Cavani, F.; Trifirò, F.; Vaccari, A. *Catal. Today* **1991**, *11*, 173. (b) Vaccari, A. *Appl. Clay Sci.* **1999**, *14*, 161.
- (2) (a) Williams, G. R.; O' Hare, D. *J. Mater. Chem.* **2006**, *16*, 3065. (b) Rives, V.; Ulibarri, M. A. *Coord. Chem.* **2002**, *12*, 3191.
- (3) Duan, X.; Evans, D. G., Eds. *Layered Double Hydroxides: Structure and Bonding*; Springer: Berlin/Heidelberg, 2006.
- (4) (a) Newman, S. P.; Williams, S. J.; Coveney, P. V.; Jones, W. J. *Phys. Chem. B* **1998**, *102*, 6710. (b) Newman, S. P.; Greenwell, H. C.; Coveney, P. V.; Jones, W. *Layered Double Hydroxides: Present and Future*; Nova Science: New York, 2001.
- (5) Newman, S. P.; Jones, W. *New J. Chem.* **1998**, *2*, 105.
- (6) (a) Fei, H.; Rogow, D. L.; Oliver, S. R. *J. Am. Chem. Soc.* **2010**, *132*, 7202. (b) Li, A.; Wang, W.; Zhu, R.; Yu, Y.; Liu, H.; Wang, S. *Biomaterials* **2011**, *32*, 469. (c) Yan, D.; Lu, J.; Ma, J.; Wei, M.; Evans, D. G.; Duan, X. *Angew. Chem., Int. Ed.* **2011**, *50*, 720. (d) Yao, H. B.; Fang, H. Y.; Tan, Z. H.; Wu, L. H.; Yu, S. H. *Angew. Chem., Int. Ed.* **2010**, *49*, 2140. (e) Wei, M.; Pu, M.; Guo, J.; Han, J.; Li, F.; Evans, D. G.; Duan, X. *Chem. Mater.* **2008**, *20*, 5169.
- (7) Greenwell, H. C.; Jones, W.; Coveney, P. V.; Stackhouse, S. J. *Mater. Chem.* **2006**, *16*, 708.
- (8) Lagaly, G.; Beneke, K. *Colloid Polym. Sci.* **1991**, *269*, 1198.
- (9) Leach, A. R. *Molecular Modeling: Principles and Applications*, 2nd ed.; Pearson Education Ltd.: England, 2001.
- (10) Mayo, S. L.; Olafson, B. D.; Goddard, W. A. *J. Phys. Chem.* **1990**, *94*, 8897.
- (11) Rappe, A. K.; Casewit, C. J.; Colwell, K. S.; Goddard, W. A. III; Skiff, W. M. *J. Am. Chem. Soc.* **1992**, *114*, 10024.
- (12) Sun, H. *J. Phys. Chem. B* **1998**, *102*, 7338.
- (13) Lifson, A.; Warshel, S. *J. Chem. Phys.* **1968**, *49*, 5116.
- (14) Cygan, R. T.; Liang, J.; Kalinichev, A. G. *J. Phys. Chem. B* **2004**, *108*, 1255.
- (15) Thyveetil, M. A.; Coveney, P. V.; Greenwell, H. C.; Suter, J. L. *J. Am. Chem. Soc.* **2008**, *130*, 12485.
- (16) (a) Lin, F.; Wang, R. *J. Chem. Theory Comput.* **2010**, *6*, 1852. (b) Lasaga, A. C.; Gibbs, G. V. *Phys. Chem. Miner.* **1987**, *14*, 107.
- (17) Shao, M.; Wei, M.; Evans, D. G.; Duan, X. *Chem. Commun.* **2011**, *47*, 3171.
- (18) Ma, R.; Liu, Z.; Takada, K.; Lyi, N.; Bando, Y.; Sasaki, T. *J. Am. Chem. Soc.* **2007**, *129*, 5257.
- (19) Pisson, J.; Morel-Desrosiers, N.; Morel, J. P.; Roy, A.; Leroux, F.; Taviot-Guého, C.; Malfreyt, P. *Chem. Mater.* **2011**, *23*, 1482.
- (20) Thyveetil, M.; Coveney, P. V.; Greenwell, H. C.; Suter, J. L. *J. Am. Chem. Soc.* **2008**, *130*, 12485.
- (21) Teppen, B. J.; Rasmussen, K.; Paul, M. B.; Miller, D. M.; Schäfer, L. *J. Phys. Chem. B* **1997**, *101*, 1579.
- (22) Hwang, M. J.; Stockfisch, T. P.; Hagler, A. T. *J. Am. Chem. Soc.* **1994**, *116*, 2515.
- (23) Maple, J. R.; Hwang, M. J.; Stockfisch, T. P.; Dinur, U.; Waldman, M.; Ewig, C. S.; Hagler, A. T. *J. Comput. Chem.* **1994**, *15*, 162.
- (24) Maple, J. R.; Hwang, M. J.; Stockfisch, T. P.; Hagler, A. T. *J. Comput. Chem.* **1994**, *34*, 195.
- (25) Peng, Z.; Ewig, C. S.; Hwang, M. J.; Waldman, M.; Hagler, A. T. *J. Phys. Chem. A* **1997**, *101*, 7243.
- (26) Chang, C. H.; Kim, K. *J. Chem. Theory Comput.* **2009**, *5*, 1137.
- (27) (a) Yu, K.; Schmodt, J. R. *J. Phys. Chem. C* **2011**, *115*, 1887. (b) Tan, O. Z.; Wu, M. C. H.; Chihai, V.; Kuo, J. L. *J. Phys. Chem. C* **2011**, *115*, 11684. (c) Perez-Angel, E. C.; Seminario, J. M. *J. Phys. Chem. C* **2011**, *115*, 6467.
- (28) Yan, H.; Wei, M.; Ma, J.; Li, F.; Evans, D. G.; Duan, X. *J. Phys. Chem. A* **2009**, *113*, 6133.
- (29) Isetti, G. *Period. Mineral.* **1965**, *34*, 327.
- (30) Merlino, S.; Orlandi, P. *Am. Mineral.* **2001**, *86*, 1293.
- (31) Allmann, R.; Jepsen, H. P. *Neues Jahrb. Mineral., Monatsh.* **1969**, *1969*, 544.
- (32) (a) Becke, A. D. *Phys. Rev. A* **1988**, *38*, 3098. (b) Lee, C.; Yang, W.; Parr, R. G. *Phys. Rev. B* **1988**, *37*, 785. (c) Vosko, S. H.; Wilk, L.; Nussair, M. *Can. J. Phys.* **1980**, *58*, 1200. (d) Becke, A. D. *J. Chem. Phys.* **1993**, *98*, 5648.
- (33) Petersson, G. A.; Al-Laham, M. A. *J. Chem. Phys.* **1991**, *94*, 6081.
- (34) (a) Frisch, M. J.; Trucks, G. W.; Schlegel, H. B.; Scuseria, G. E.; Robb, M. A.; Cheeseman, J. R.; Scalmani, G.; Barone, V.; Mennucci, B.; Petersson, G. A.; Nakatsuji, H.; Caricato, M.; Li, X.; Hratchian, H. P.; Izmaylov, A. F.; Bloino, J.; Zheng, G.; Sonnenberg, J. L.; Hada, M.; Ehara, M.; Toyota, K.; Fukuda, R.; Hasegawa, J.; Ishida, M.; Nakajima, T.; Honda, Y.; Kitao, O.; Nakai, H.; Vreven, T.; Jr. Montgomery, J. A.; Peralta, J. E.; Ogliaro, F.; Bearpark, M.; Heyd, J. J.; Brothers, E.; Kudin, K. N.; Staroverov, V. N.; Keith, T.; Kobayashi, R.; Normand, J.; Raghavachari, K.; Rendell, A.; Burant, J. C.; Iyengar, S. S.; Tomasi, J.; Cossi, M.; Rega, N.; Millam, J. M.; Klene, M.; Knox, J. E.; Cross, J. B.; Bakken, V.; Adamo, C.; Jaramillo, J.; Gomperts, R.; Stratmann, R. E.; Yazyev, O.; Austin, A. J.; Cammi, R.; Pomelli, C.; Ochterski, J. W.; Martin, R. L.; Morokuma, K.; Zakrzewski, V. G.; Voth, G. A.; Salvador, P.; Dannenberg, J. J.; Dapprich, S.; Daniels, A. D.; Farkas, O.; Foresman, J. B.; Ortiz, J. V.; Cioslowski, J.; Fox, D. J. *Gaussian 09*, revision B.01; Gaussian, Inc.: Wallingford CT, 2010. (b) Rauhut, G.; Pulay, P. *J. Phys. Chem.* **1995**, *99*, 3093.
- (35) Berendsen, H. J. C.; Postma, J. P. M.; van Gunsteren, W. F.; Hermans, J. Interaction models for water in relation to protein hydration. In *Intermolecular Forces*; Pullman, B., Ed.; D. Reidel: Amsterdam, 1981.
- (36) Yan, D.; Lu, J.; Wei, M.; Li, H.; Ma, J.; Li, F.; Evans, D. G.; Duan, X. *J. Phys. Chem. A* **2008**, *112*, 7671.
- (37) Allen, M. P.; Tildesley, D. J. *Computer Simulation of Liquids*; Clarendon: Oxford, U.K., 1987.
- (38) Andersen, H. C. *J. Chem. Phys.* **1980**, *72*, 2384.
- (39) Parrinello, M.; Rahman, A. *J. Appl. Phys.* **1981**, *52*, 7181.
- (40) Blomberg, L. M.; Mangold, M.; Mitchell, J. B. O.; Blumberger, J. *J. Chem. Theory Comput.* **2009**, *5*, 1284.
- (41) Peters, M. B.; Yang, Y.; Wang, B.; Füsti-Molnár, L.; Weaver, M. N.; Merz, K. M. Jr. *J. Chem. Theory Comput.* **2010**, *6*, 2935.
- (42) Nilsson, K.; Lecerof, D.; Sigfridsson, E.; Ryde, U. *Acta Crystallogr.* **2003**, *59*, 274.
- (43) Hill, J. R.; Sauer, J. J. *Phys. Chem.* **1994**, *98*, 1238.
- (44) Hill, J. R.; Sauer, J. J. *Phys. Chem.* **1995**, *99*, 9536.
- (45) (a) Torczon, V. *SIAM J. Optim.* **1997**, *7*, 1. (b) Müller, C. W.; Newby, J. J.; Liu, C. P.; Rodrigo, C. P.; Zwier, T. S. *Phys. Chem. Chem. Phys.* **2010**, *12*, 2331. (c) Ryan, P. M.; Teague, L. C.; Meehan, D. E.; Boland, J. J. *J. Am. Chem. Soc.* **2011**, *133*, 14287. (d) Li, H.; Ma, J.; Evans, D. G.; Zhou, T.; Li, F.; Duan, X. *Chem. Mater.* **2006**, *18*, 4405.
- (46) Lombardo, G. M.; Pappalardo, G. C. *Chem. Mater.* **2008**, *20*, 5585.
- (47) (a) Pertlik, F. *Monatsh. Chem. Verw. Teile Anderer Wiss.* **1999**, *130*, 1083. (b) Cairns, R. W.; Ott, E. *J. Am. Chem. Soc.* **1933**, *55*, 527. (c) Baneeva, M. I.; Popova, S. V. *Geokhimiya* **1969**, *1969*, 1014.
- (48) (a) Xu, Z. P.; Zeng, H. C. *J. Phys. Chem. B* **2001**, *105*, 1743. (b) Roussel, H.; Briois, V.; Elkaim, E.; de Roy, A.; Besse, J. P. *J. Phys. Chem. B* **2000**, *104*, 5915. (c) Johnsen, R. E.; Krumeich, F.; Norby, P. *J. Appl. Crystallogr.* **2010**, *43*, 434. (d) Hansen, H. C. B.; Kock, C. B.; Taylor, R. M. *J. Solid State Chem.* **1994**, *113*, 46. (e) Han, Y. F.; Li, H. J.; Ma, X. G.; Liu, Z. H. *Solid State Sci.* **2009**, *11*, 2149.
- (49) Shannon, R. D. *Acta Crystallogr.* **1976**, *A32*, 751.
- (50) Born, M.; Huang, K. *Dynamical Theory of Crystal Lattices*; Oxford University Press: London, 1954.
- (51) Mitra, S. S. *Solid State Phys.* **1962**, *13*, 1.
- (52) Braterman, P. S.; Cygan, R. T. *Am. Mineral.* **2006**, *91*, 1188.

- (53) Ugliengo, P.; Zicovich-Wilson, C. M.; Tosoni, S.; Civalleri, B. *J. Mater. Chem.* **2009**, *19*, 2564.
- (54) Dawson, P.; Hadfield, C. D.; Wilkinson, G. R. *J. Phys. Chem. Solids* **1973**, *34*, 1217.
- (55) Lutz, H. D.; Moller, H.; Schmidt, M. *J. Mol. Struct.* **1994**, *328*, 121.
- (56) Kloprogge, J. T.; Wharton, D.; Hickel, L.; Frost, R. L. *Am. Mineral.* **2002**, *87*, 623.
- (57) Zhu, H.; Huang, S.; Yang, Z.; Liu, T. *J. Mater. Chem.* **2011**, *21*, 2950.